# Accepted Manuscript

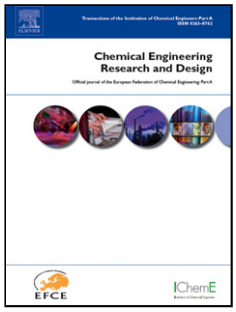


Title: Effect of residence time and energy dissipation on drop size distribution for the dispersion of oil in water using KMS and SMX+ static mixer

Authors: G. Forte, E. Brunazzi, F. Alberini

PII: S0263-8762(19)30303-X
DOI: https://doi.org/10.1016/j.cherd.2019.06.021
Reference: CHERD 3719

To appear in:

Received date: 31 October 2018
Revised date: 12 June 2019
Accepted date: 13 June 2019

Please cite this article as: Forte G, Brunazzi E, Alberini F, Effect of residence time and energy dissipation on drop size distribution for the dispersion of oil in water using KMS and SMX+ static mixer, *Chemical Engineering Research and Design* (2019), https://doi.org/10.1016/j.cherd.2019.06.021

# Effect of residence time and energy dissipation on drop size distribution for the dispersion of oil in water using KMS and SMX+ static mixer

G. Forte[a,b], E. Brunazzi[b], F. Alberini[a*]

[a] School of Chemical Engineering, University of Birmingham, B15 2TT, K;

[b] Dipartimento di Ingegneria Civile e Industriale, University of Pisa, Via Dio Ti Salvi, Italy;

* Corresponding author: Dr Federico Alberini, School of Chemical Engineering, University of Birmingham, B15 2TT, UK; Email f.alberini@bham.ac.uk.

Research Highlights

- Characterisation of in-situ drop size Oil in Water emulsion is presented.
- Optical and PLIF measurements and image analysis were used to determine the DSD
- Consistent instabilities were observed for all configurations at *Reynolds* above 6000.
- Existing models showed good agreement with the experimental data in stable conditions.
- Existing models were tested which showed poor agreement in the unstable conditions.

**Abstract**

The Planar Laser Induced Fluorescence technique was used to determine the drop size distribution of oil dispersed in water at the inlet and outlet of two static mixer geometries (KMS and Sulzer_SMX+) equipped with either 6 or 12 elements. A mineral oil (Lytol®), three times more viscous than the water continuous phase, was used as the dispersed phase. The oil flow rate was kept constant through all experiments forcing the drop detachment from the secondary inlet. The L-L system was very dilute (~0.05-0.0007% v/v O/W) to avoid coalescence phenomena. The flowrate of the continuous phase (water) was altered giving values of Reynolds number from 2,000 to 12,000, covering high transitional and turbulent flow regimes. Increasing the flow rate of the continuous phase, the detached oil drops from

the secondary inlet decreased in size as expected. However, same drops after flowing a length of 0.4 m of an empty pipe reached a constant size. To investigate a wider range of energy dissipation and residence time, the presence of static mixers has been investigated. Pressure drops, hence energy consumed, were measured to compare the different set ups and drop size distributions. The results show that by increasing the flow rate, the drop size decreased up to a critical point, beyond which oil droplet size reduction became inefficient. The collected data were then used to derive a methodology to identify the optimal flow conditions and choice of static mixer device to achieve best drop size reduction with less energy per unit mass.

**Keywords:** liquid-liquid mixing, PLIF, static mixer, droplet breakup

# 1. Introduction

The dispersion of one liquid into another is a key process step in creating emulsions in many industry sectors including oil, food processing, fast moving consumer goods (FMCG) and pharmaceuticals [1–6]. Academic research in this area is driven by gaining an understanding of the fundamental mechanisms of drop breakup and the requirements to stabilise the resulting dispersion to form an emulsion. The industry driver is the control of emulsion microstructure which is a critical quality attribute in manufacture. This is further complicated by the choice of emulsifier, (usually a surfactant) which is critical in both emulsion formation and long-term stability, as emulsions are inherently not thermodynamically stable [7]. Emulsions can be categorised [8] as oil-in-water (O/W), water-in-oil (W/O), oil-in-oil (O/O) and aqueous two-phase systems [9]. These systems are normally made up of a dispersed or drop phase and a continuous or matrix phase, in which the dispersed phase is commonly smaller in volume than the continuous phase [10].

Commonly, significant energy addition is required to generate droplets [11, 12] and the smaller the droplets become, the more energy is required. The reduction in interfacial tension and change in interfacial mobility afforded by the addition of the surfactants promotes droplet formation, even at low concentrations [13]. Drop formation is mainly driven by the Kelvin-Helmholtz instability [14], a phenomenon that takes place when two fluids of different densities move in parallel flows [15]. This is a key mechanism which is found in many

applications involving interface interaction such spray formation by pre-filming atomizers [16].

Fundamental research on emulsions is continually expanding due to the increasing demand for complex models [17] which require a deep understanding of physical chemistry as well as knowledge of the manufacturing processes. A critical step is scaling up from lab to industrial scale, which is an ongoing challenge for industry in terms of feasibility and environmental impact and for academia in gaining understanding of the underlying physics. Thus, it is vital to identify the key mechanisms to develop successful and innovative process scale ups with enhanced controllability.

An increasing driver for industry is the use of continuous processes rather than conventional batch processes, due to consequent reduction in plant footprint, fluid inventory and the cost of the requirement for improved on or at-line measurements of product quality or process control. Inline mixing and drop breakup can be achieved by use of a static mixer device, which consists of a pipe containing shaped inserts which promote mixing; thus static mixers divide and redistribute streamlines in a sequential fashion using the pumping energy of the flowing fluid [18–21]. Emulsification in static mixer systems has been extensively studied for concentrated emulsions using off line Drop Size Distribution (DSD) measurements [14, 22, 23]. Lobry et al. [24] compared offline and online measurements using a Mastersizer and an online Turbiscan showing the advantages and the disadvantages of the two methodologies.

The work presented in this paper is an investigation of droplet breakup of a dispersed oil phase in water obtained by using two geometries of static mixer, namely the Kenics® KMS mixers (Chemineer, USA) and SMX+® (Sulzer) designs. The size of the drops was obtained using inline Planar Laser Induced Fluorescence (PLIF) applied at the outlet of the mixer. This technique was adapted from the method used by Alberini et al. [25] to obtain striation distributions in miscible fluid mixing in static mixers; this is extended to immiscible systems by doping the dispersed phase with a fluorescent dye as used by Liu et al. [26] in co-current flow in a vertical pipe. The experiments were carried out at a low concentration of the dispersed phase in the high transitional and turbulent regimes. Investigations were made on the effect of viscosity ratio between the dispersed and the continuous phase, and on the number of mixing elements. On the basis of the results obtained, a interfacial energy model is proposed which is tested against the experimental data.

# 2. Material and methods

## 2.1 Experimental Rig

Figure 1a shows the overall schematic of the experimental rig. The primary flow, water doped with fluorescent dye was delivered by a Liquiflo gear pump controlled using a motor drive (Excal Meliamex Ltd) and monitored using an electromagnetic flow meter (Krohne). The secondary flow, oil doped with Nigrosine dye, was introduced using a syringe pump (Harvard PHD 2000). The secondary flow was injected into the system through a needle, with an internal diameter of 1 mm, located in the centre of the pipe section and placed as close as possible to the first mixer element. The flow rate of the secondary flow was kept constant for all runs ($8\times10^{-9}$ $m^3$ $s^{-1}$). The range of volume ratio between dispersed and continuous phase was between 0.05 to 0.0007%.

KMS and SMX+ static mixers of internal diameter (ID) $12.7\times10^{-3}$ m (1/2") were used, equipped with either 6 (length of 0.095 m for SMX+ and 0.135 m for KMS) or 12 (0.190 m for SMX+ and 0.270 m for KMS) mixing elements. A Tee-piece (Figure 1b) was placed at the end of the mixer section and a glass window was inserted in the corner of the Tee piece, normal to the axis of the main pipe flow. This enabled visualisation of the cross section of the pipe using PLIF. The distance from the window and the laser sheet was 0.07 m. A glass pipe, built inside a glass box, was located upstream of the Tee after the static mixer outlet. This provided the optical access for the laser sheet to illuminate the cross section of the pipe. Differential pressure sensors were located both upstream and downstream of the static mixer section, enabling measurement of the pressure drop at a sampling rate of 5 Hz. The sensors were placed as close as possible to the mixer section, mounted four pipe diameters before and after the section respectively. Pressure drop data was obtained for each experiment over a range of superficial velocities from $0.1 < V < 0.9$ m $s^{-1}$ ($0.16 \cdot10^{-4} < Q < 11.3 \cdot10^{-4}$ $m^3$ $s^{-1}$). A relief valve with a maximum pressure of 3 bar was installed for safety reasons after the main pump. In this work the refractive index matching technique was not applied because did not help on the clear recognition of oil dispersed drops in the continuous phase hence a different strategy was used.

The primary flow was a solution of water and fluorescent dye (Rhodamine 6G, $5\cdot10^{-4}$ kg $m^{-3}$). The secondary flow was Lytol, a low viscosity oil ($\mu = 0.0032$ Pa s) containing a non-ionic

surfactant sorbitane monooleate (Span80 0.5% w/w ([27])) and Nigrosine black dye (of $1 \cdot 10^{-4}$ kg $m^{-3}$); the use of fluorescent (water) and Nigrosine (oil) dyes together increased the contrast between the continuous (high grey scale values) and the dispersed phases (very low grey scale values) hence the refractive index matching technique. This combined strategy helped the image processing step where shadows of drops crossing the laser plane and out of focus drops were not considered in the analysis. Generally, the gradient of grey scale values between shadows and drops was in the order of 100 (12bit image hence 4096 grey scale values). Furthermore, the high grey scale values of the continuous phase helped to dilute the contrast of oil drops once they had passed the focus plane. The temperature of the fluids was monitored and maintained at 23 °C to ensure that fluid rheology, well described by the Newtonian model, remained constant. In Table 1, properties of the fluids are reported.

## 2.2 Optical measurements

Two optical measurements were conducted: high speed photography for droplet formation and PLIF for droplet size detection. Both were used to monitor the change in droplet size using a fixed dispersed phase injection flow rate and varying the Reynolds (*Re*) number of the continuous phase.

The first measurement was carried out using a Photron FASTCAM SA3 high speed camera and had the objective of capturing the oil drops as they formed at the outlet of the injection needle in the case of empty pipe, to guarantee the optical access to the needle area. The acquisition rate was 500 frames per second (fps) with 1 Mega pixel resolution (1000 × 1000 pixels). For each flow rate (of the continuous phase) several oil drops were recorded and measured using Image J software.

The second measurement consisted in PLIF combined with image processing, which was used to calculate the values of $d_{32}$ at the outlet of the pipeline with and without (empty pipe) the static mixer at different flow rates. The cross section of the tube was illuminated by the laser which contrasted the oil drops against the water (doped with fluorescent dye). The 2-D PLIF measurements were performed using a TSI PIV system (TSI Inc., USA). The system comprised of a 532 nm Nd-Yag laser (Litron Nano L50 100) pulsing at 7 Hz, synchronized to a single TSI Powerview 4MP (2048 × 2048 pixels) 12 bit CCD camera using a synchronizer (TSI 610035) attached to a computer. The PIV system was controlled using TSI Insight 4G software. The camera was equipped with a 545 nm cut-off filter to eliminate reflected laser

light so that only the fluorescent light emitted by the dye, excited in the measurement plane, was captured in the image. The spatial resolution of the measurements was 10 μm·pixel$^{-1}$ which allowed the detection of drops in the order of 20 μm diameter (2x2 pixel detection). The whole range of experimental setups, such as selection of flow rates and static mixer lengths have been selected in order to work in a "detection confident zone" of the oil drops (minimum drop size reached was ~40 μm and the area frequency do not exceed 0.02%) within the experimental limitations.

For all optical measurements, the glass pipe was surrounded by a glass cubic box filled with distilled water in order to offer to the laser sheet a perpendicular plane to hit, reducing the aberrant effect of the curved surface of the pipe. The acquired raw images were processed as described in section 2.3.

## 2.3 Image processing

The drop sizes were obtained by processing the raw PLIF images using MATLAB scripts. The image processing consisted of four main steps (summarised in Figure 2):

1. Capture of raw images: 12-bit images (2048 × 2048 pixels) were captured by the PIV system. To ensure statistical validity of the drop size measurements, 500 images were captured for each run. Full details are disclosed in the paragraph 2.4.
2. Filtering raw images: to enhance the quality of the images and to aid processing, a smooth Gaussian filter was used to remove background noise while keeping the dimension of the drops constant. As a result, drops outside of the focal plane were eliminated.
3. Selection of drops: the segmentation function of DipImage MATLAB toolbox was used to select and recognise the oil drops (discarding drops in touch with the wall). The image was then binary gated.
4. Labelling and calculating drop size diameters: each drop was recognized labelled and measured (area, perimeter and diameter) in turn.

This analysis was repeated for the 500 acquired images for each velocity and each configuration (6-12 elements SMX+, 6-12 elements KMS and the empty pipe). The processing time was minimal, < 0.5 s, for each image. The resulting matrices from image analysis were then processed to obtain the DSD in terms of area frequency.

### 2.4 Statistical analysis

To evaluate the repeatability and the consistency of the method, a series of DSD graphs were plotted which represent how the DSD changes as a function of the number of images processed: 100, 200, 300 and 500 (an example is reported in Figure 3). The comparison was carried out at different velocities and static mixer devices which always give consistent results after 100 images.

However, to verify the reliability of results in terms of statistical analysis, a more detailed investigation was done based on the approach described in Buffo and Alopaeus' [28] work. Their theoretical approach was used for the determination of the optimal sample size, after a small preliminary sampling. This procedure was applied to establish the connection between the number of measurements necessary to ensure a certain level of confidence in a fixed confidence interval ΔL, considering $\bar{L}$, the average size value for each static mixer setting. In Table 2, the values of N, the number of drops detected for each experimental run and all parameters required to determine $N^*$ (the desired number of measured drops to achieve a 99% level of confidence) are presented. The confidence interval ΔL was chosen according to the resolution of the camera and the measured minimum drop size (ΔL=0.03 mm). To calculate $N^*$, the parameters $t_\infty$ (t value for infinite degrees of freedom of a two-tail student's t-distribution), $\sigma_{SE}$ (standard deviation calculated from S and $\sqrt{N}$) and $S^2$ (variance of the sample) were also evaluated. The analysis was carried out for mono-modal and bi-modal distributions for different static mixer geometries. In addition, the analysis was carried out for all runs at different velocities, but only the results for selected velocities (a subset of all results) are presented in Table 2. All the values of $N^*$ are lower than N values which verify the reliability of the acquired results.

## 3. Theory

Drop breakup occurs when the external stresses overcome the Laplace pressure. Laplace pressure is the difference in pressure between the convex and the concave sides of the curved interface of a droplet. The deformation of the drop requires high external stress, and this implies a very large pressure gradient. The stress is due to a velocity gradient or to a pressure difference arising from inertial effects [29]. Naming those external stresses as $\tau$, the droplet breaks if:

$$\tau > \frac{2\sigma}{R}, \qquad \text{Eq. (1)}$$

where σ is the interfacial tension and R the size of the drop.

The ratio of disruptive forces to cohesive stresses is known as critical Weber number (We) in the case of turbulent flow.

$$We_{crit} = \frac{\rho_c <u'^2> d_{32}}{\sigma} \qquad \text{Eq. (2)}$$

The velocity fluctuation *u'* is,

$$u' \equiv (\varepsilon\, \lambda)^{\frac{1}{3}}. \qquad \text{Eq. (3)}$$

The flow regime is indicated by the value of the Reynolds number:

$$Re = \frac{\rho\, u\, l}{\mu_c} \qquad \text{Eq. (4)}$$

Where $\rho$ is the density, $u$ the superficial velocity, $l$ the characteristic length (diameter of the static mixer) and $\mu_c$ the viscosity of the continuous phase.

It is a well-known theory [30] that in the turbulent regime, an energy cascade causes the transfer of kinetic energy from the largest eddies (of the order of pipe diameter) to the smaller eddies, which in the end dissipate it as friction at the Kolmogorov scale. These same eddies apply a stress to the drops causing deformation that may lead to droplet breakup, following different mechanisms depending on the relative size of drops and the smallest eddies. If the drops are larger than Kolmogorov length scale, they are disrupted by the inertial pressure/velocity fluctuation across the drop; otherwise when the droplets are smaller than Kolmogorov's scale, the mechanism is due to laminar shear stresses.

It has also been observed [31] that together with the magnitude of the disruptive stress, it is important to consider the breakup time $t_b$. For breakup time is meant the time spent by a drop in a fixed volume at a given average dissipation energy. Works in the literature report it to be proportional to the diameter of the droplet $d$ and the average dissipation energy $\varepsilon$:

$$t_b \sim d^a \varepsilon^b \qquad \text{Eq. (5)}$$

However, different numbers and even different signs are found in the literature, e.g. values of $a$ range between -2/3 and 2/3, and $b$ between -1/3 and -2/3 [32–34]. It is thus not clear if the diameter of the droplets has a positive or negative effect on the time needed for the breakup. This time $t_b$, is the time needed for the turbulence to interact with the droplet and cause deformation, and for a consequent step of internal flow mechanism inside the droplet [35] to take place, that would finally cause the disruption. Ashar et al. [31] have also studied a

probability function of breakup that is found to increase monotonically with the Weber number (*We*). Getting to the breakup condition is also dependant to the probability that a droplet finds itself in a location of higher instantaneous stress [36]. Especially for dilute systems and single droplets observations, mechanisms and results of droplet breakups are to be related not only to the energy dissipation but also to the residence time at such state, which would increase the probability of it to encounter higher instantaneous stress conditions. Other studies have focused on the number of fragments resulting from droplet breakup, concluding that binary breaking it is not the most common [37] and to determine experimentally the breakup frequency [38].

Due to the scale of the smallest droplets in this work, all breakup is assumed to occur by turbulent inertial breakup. Thus, the external stress is proportional to velocity fluctuations and from Hinze [38], the velocity fluctuations can be related to the energy dissipation rate [39], $\varepsilon$, that for a motionless mixer [40, 41] is:

$$\varepsilon = \frac{\Delta P_{sm}\, Q}{\rho\, A\, l}, \qquad \text{Eq. (6)}$$

where $\Delta P_{sm}$ is the pressure drop of the static mixer, $Q$ the flow rate and $A$ is the cross-section of the pipe. Then, knowing that a large spectrum of eddies length ($\lambda$) is:

$$\lambda \equiv \nu_c^{3/4} \varepsilon^{-\frac{1}{4}}. \qquad \text{Eq. (7)}$$

Rearranging the formula, it is possible to find a correlation between the maximum drop size and the dissipation rate:

$$d_{32} = C_x \left(\frac{\sigma}{\rho}\right)^{0.6} \varepsilon^{-0.4} \qquad \text{Eq.(8)}$$

with $C_x \approx 0.725$ using $d_{max}$ instead of $d_{32}$ [38].

In the literature, there are several models which relate the Sauter diameter, $d_{32}$, with the Re and We numbers for static mixers. Many of the models in the literature show only different values of the constant which can be used for fine tuning of the model, but this is not the main objective of this work. The following models are used to show the general trends and to compare experimental data with theoretical results.

The first model was proposed by Streiff [42]; the value of $C_x$ is estimated as 0.2 where $d_{max} = 1.5\, d_{32}$.

$$d_{max} = C_x \left(\frac{\sigma}{\rho_c}\right)^{0.6} \left(\frac{\rho_c}{\rho_d}\right)^{0.2} \varepsilon^{-0.4} \qquad \text{Eq. (9)}$$

The second model, proposed by Poncelet and Neufeld [43], has a different constant ($C_z$=1.2) and an additional term to take into account the viscosity ratio between the continuous and dispersed phases.

$$\frac{\bar{d}}{D} = C_z\, We^{0.65}\, Re^{0.2} \left(\frac{\mu_d}{\mu_c}\right)^{0.5} \qquad \text{Eq. (10)}$$

where $\bar{d} = C_{zx} d_{max}$ and $D$ is the diameter of the pipe.

For this work $d_{32}$was used in the correlations instead of $\bar{d}$ in order to eliminate the constant $C_{zx}$which is not known. This has been done assuming that $d_{32}$ is proportional to $d_{max}$. In this work eq. (10) is modified as:

$$\frac{d_{32}}{D} = C_{z_{32}} We^{0.65}\, Re^{0.2} \left(\frac{\mu_d}{\mu_c}\right)^{0.5} \qquad \text{Eq. (11)}$$

## 3.1 Energy model

The dispersed droplet diameter is affected by the energy input into the system which can be measured by the pressure drop. However, not all the energy input contributes to drop breakup. Most of the energy is lost as heat (due to friction) or converted into momentum for phase contacting (hydrodynamic mixing) [44]. Furthermore, it is possible to estimate the potential energy (or interfacial energy ($E_{sur}$)) which a droplet needs for the breakup. This energy can be defined as:

$$E_{sur} = \pi\, \sigma\, d^2 \qquad \text{Eq. (12)}$$

At fixed interfacial tension $\sigma$, the larger the diameter $d$ of the droplet , the higher the interfacial energy. Using the DSD, an average interfacial energy was estimated by summing over all drops to determine

$$E_{sur} = \pi\sigma \sum_{n}^{i=1} {d_i}^2\, N_i \qquad \text{Eq. (13)}$$

Where $d_i$ are the diameter range values of the DSD and $N_i$is the total number of drops per $d_i$.The change in interfacial energy associated with the droplet breakup, $\Delta E_{sur}(d_i)$ can thus be calculated as:

$$\Delta E_{sur} = E_{sur}^{inlet} - E_{sur}^{outlet} \qquad \text{Eq. (14)}$$

and then compared with the power input. Where, the inlet superscript corresponds to the mother drops and outlet to the DSD after passing through the static mixer for the fixed time of a single PLIF measurements which correspond to 71 seconds. Finally, a dimensionless fractional change $Y$ can be defined as:

$$Y = \frac{E_{sur}^{inlet} - E_{sur}^{outlet}}{E_{sur}^{inlet}} \quad \text{Eq. (15)}$$

This value can be used to facilitate the understanding of the results of the oil droplet dispersions; it can be thought of as a rate of dispersion where the drops are theoretically getting smaller increasing the power input into the system.

Using this concept, it is possible to extrapolate a simplistic model, which can help to understand the dynamics of the droplet breakup; a single large drop enters the mixing system where it is exposed to destabilising stresses due to the energy input $E_{ext}$ by the pump which is applied to the system,

$$E_{ext} = \frac{\Delta P_{sm}}{\rho} \quad \text{Eq. (16)}$$

where $\Delta P_{sm}$ is the pressure drop within the static mixer and $\rho$ is the density of the continuous phase. Similarly, the power input per unit mass is defined as:

$$P = \frac{\Delta P_{sm}\, u}{\rho\, L_{sm}} \quad \text{Eq. (17)}$$

Where, the additional terms $u$ and $L_{sm}$ are the superficial velocity of the continuous fluid and length of the static mixers respectively (thus the ratio between $L_{sm}$ and $u$ is the mean residence time). The length of the static mixer changes with the type of mixer and number of elements.

# 4. Results

## 4.1 Drop size characterisation

The formation of droplets at the tip of the needle was observed at different flow rates of the continuous phase. The droplet formation mechanism was not investigated in this work, but it has been observed that the elongation and breakage of the drop formed at the outlet of the needle, often, but not always, resulted in a binary breakage. The formation of multiple satellite droplets beside the main drop was common especially increasing *Re* of the primary flow. In Figure 4, images showing the different observed phases of droplet formation in the case of binary breakage are reported at three Reynolds number. In the first time-step, the drop is forming outside the needle and it increases in size as more oil is fed through the needle. In time step 2, there is an elongation that brings to breakage. The image acquired at time step 3

immediately follows the previous one and a second small droplet is formed from the tail of the main drop as it detaches from the needle. The last condition sees the two droplets moving away from the injection pipe; in this image is possible to appreciate the reduction in size of the drops at higher *Re*, when the higher stress offered by the main flow one the forming droplet, causes an earlier detachment from the inlet pipe.

This phenomenon is observable also in Figure 5, where the initial diameter $d_{IN}$ (estimated from the series of images similar to the selected one shown in Figure 4) is reported at different *Re* in comparison with "empty pipe" $d_{32}$. The last values were obtained applying PLIF to an empty (not equipped with static mixers) pipe long 0.43 m, following the image processing procedure described in 2.3. The length of the pipe was chosen to achieve pressure drops above the sensitivity of the pressure sensors. It can be noted that, although the formed droplets differ in size at the start, after being subject to the stress applied by the turbulent flow, their size reach similar values at all operating *Re.* The measurement of the satellite droplet was included in the calculation of $d_{IN}$. It has been assessed that the minimum size diameter of such droplets obtained is in the order of 0.08 mm.

Figure 6 shows the DSDs at different *Re* numbers (from 2000 to 12000) using 12 elements SMX+. Unsurprisingly, at *Re* between 2000 and 6000, the DSDs mean move towards left (the overall drop size decreases) as the energy input increases. The flow regime is assumed to be turbulent throughout; Hirech [45] and Reynolds [46] report that the critical value of *Re* to reach the turbulent regime in a static mixer is lower (between 1500 to 3000) compared to an empty pipe due to the complex flow trajectories caused by the device geometry. However, in the range of *Re* between 6000 and 12000 (DSDs in red), the trend is not as expected as the DSD shifts towards the right at larger drop ranges with the increase of *Re*. Furthermore, the distribution also becomes bimodal instead of mono-modal which suggests that instabilities occur at higher Reynolds numbers. The higher the *Re,* the higher the secondary peak (at larger drop size) gets at the expenses of the expected peak at lower DSD mean value, up to a point at which the distribution goes back to be mono-modal, but at larger droplet size.

Comparing the obtained bimodal distributions with the initial measured diameters it is possible to relate the larger droplet size to the initial size of the droplets $d_{32}$ (Figure 5) and instead the smaller droplet size to the minimum measured diameter of the satellite drops. This suggests that both residence time and energy dissipation play an important role. The results,

in fact, show that at lower *Re* number, the droplets reach zones of high energy (hot spots) dissipation for enough time. Increasing the flow rate (up to *Re*=6000), the overall DSD shifts to the left which suggests that the energy dissipation increases, and the combination of flow and length of the static mixer allows to reach a resident time long enough to cause breakup of the drop. However, increasing even more the flow rate, this is not the case anymore. Thus, even if the energy dissipation increases, the residence time decreases down to a level which does not allow the drop to break. Indeed, although the system is running at steady state conditions, increasing the flow rates causes the drop to spend less time in the fixed volume of the mixing zone (volume of the empty pipe-volume of the static mixer frame).

The Kolmogorov length scale ($\lambda$) is ~$2 \times 10^{-5}$ m and ~$4 \times 10^{-5}$ m at *Re* = 12,000 and *Re* = 5,000 respectively. These estimations were obtained using the physical properties of the continuous phase. In both cases, the obtained drop sizes were larger than the Kolmogorov scale, therefore it is unlikely that a transition between the inertial subrange and the turbulent viscous regime would take place. On the basis of the breaking time theory [31] described in section 3, a possible explanation is that at higher *Re*, and therefore at higher $u$, the droplets do not spend enough time at the high stress condition and therefore, although more energy is input in the system, a lower performance is achieved. As an example, at the highest *Re* in the 12 elements SMX+ static mixer, the average residence time is 0.2 s (calculated from the volume of the mixing zone in the static mixer within the 12 elements divided by the volumetric flow rate) while the breakup time $t_b$ is can vary according to the diameters of the droplets and of course of the exponent chosen for equation (5). Hence, it is plausible that the time spent by the droplet, in the static mixer device does not allow the breakup to occur, or to repeatedly occur (breakup can occur more than once).

From the acquired experimental results, this behaviour was noticed for both geometries and length of static mixer used. Figure 7 shows the DSDs for the different set ups and at three characteristic Reynolds numbers (5000, 8000, 12000). Comparing the different geometries of static mixer at constant number of elements ((a) SMX+ 12 elements with (b) KMS 12 elements and (c) SMX+ 6 elements with (d) KMS 6 elements) the SMX+ performs better at Re=5000 but beyond this, at high *Re*, the difference in performance between the two devices is not significant.

Comparing the same devices but with different number of elements (Figure 7a with c and b with d), a reduced drop size at *Re*=5000 can be observed with the increase of number of elements; instead, looking at the influence of the *Re* number at a fixed setup, not significantly

better performance are achieved increasing *Re*, suggesting that the system is not working in an efficient way.

These unstable conditions within the turbulent regime for very dilute dispersions have not been previously discussed in the literature. The use of a low fraction of oil in water avoids any effect of coalescence and also gives fewer restrictions to the trajectories of the oil drops in the static mixer device. In Table 3, measured pressure drop ($\Delta P$, [Pa]), calculated energy dissipation from Eq. (6) ($\varepsilon$, [$m^2$ $s^{-3}$]) and Reynolds number (*Re*, [-]) are presented for selected superficial velocities ($u$, [m $s^{-1}$]) at the inlet of the used static mixers (12 KMS, 12 SMX+, 6 KMS, 6 SMX+).

## 4.2 Comparison of experimental data with existing DSD models

Existing models were compared with the $d_{32}$ results obtained from the online measurements. The Hinze model (8) was fitted to the data of $d_{32}$ versus energy dissipation in Figure 8a. The data fit reasonably well until the critical point is reached, which was discussed previously. In this case, for $\varepsilon$ higher than 6 $m^2$ $s^{-3}$, a different behaviour is observed.

Altered trends are shown in Figure 8a; for shortest residence times (6 elements KMS and SMX+) the results disagree with the Hinze model which does not take into account the effect of the breakup kinetics. Different trend is show for the 12 elements static mixer (KMS and SMX+) which disagree as well with Hinze model only high energy dissipation but with a different degree compared to the 6 elements (KMS and SMX+).

To further prove this concept, as presented in Section 3, two other common models have been tested (Streiff [42] and Poncelet [43]) where the first one is independent of the viscosity ratio but take into account the density ratio and the latter instead is the other way round. Again, the measured values of $d_{32}$ were fitted using the models and the data are shown in Figure 8b. The constants obtained for the two models were $C_x$=0.2 and $C_{z32}$=0.3. The two models fit reasonably well with the experimental data (below *Re*=8000), but do not describe the different trend of the Lytol oil at high *Re*. This work does not want to invalidate previous models but to draw attention to the effect of residence time. Existing models show to be effective when the break up is mainly affected by the energy dissipation in systems where the residence time is not a limiting step. Another observation is that the introduction of viscosity ratio (even if the values are a few orders of magnitude different) does not significantly change the model predictions much between the Streiff and Poncelet models.

In the last section of this work, a methodology to determine optimal operating conditions for static mixers, is proposed. This method is based on integrating data acquirable on plant with predetermined detailed micro properties of the product.

### 4.3 Energy consumption versus Energy required for breakup

An approach to determine performance of static mixers towards oil droplet breakup is presented in this work. In Figure 9, the power input (eq.17) versus *Re* is plotted. General trends show that power increases with *Re*, and at a given *Re*, SMX+ dissipates more power than KMS, as expected, because the pressure drops are higher.

However, for a fair comparison, the performance was also compared at same energy input. The energy consumption depends on the number of mixing elements and flow rate; the fewer the elements and lower flow rate, the lower the energy consumption is, as expected. This can lead essentially that the residence time in the static mixers, can be combined with DSD information obtained from the PLIF measurement, to establish what is the optimal operating point.

To integrate the DSDs information requires a further step in the analysis. Referring to the energy model discussed in 3.1, the rate of drop breakup, Y, (defined in eq. (15)) can be plotted versus the power input (Figure 10). The information reported in this plot can be used to choose both the more suitable geometry and process conditions. The data acquired shows a plateau of rate after specific values of power according to the static mixer used (length and geometry), beyond which there is a drastic drop in breakup rate increase: this point corresponds to the critical point where the system starts switching towards a bimodal DSD. The ideal working condition is identified at the maximum achievable Y, where the highest amount of energy input in the system is used for the droplet breakup. In the plot, for each configuration, the green lines identify the power input values at which the efficiency Y decreases below the value of 0.92, identified as the critical value below which the instability is observed. This information can be used to identify the optimal working condition in Figure 9.

In support of the proposed method, two case studies are presented to show how this analysis can be used to identify the optimal operating condition. In both Figure 11a and Figure 11b, the green line identifies the critical point for the used oil in each static mixer setup (the maximum power input after which the efficiency drops below an ideal value of 0.92 as identified in Figure 10). The region to the left of the green dotted line is the “efficient

working zone", while the region on its right is named as "inefficient working zone". The performance comparison is done at fixed energy input, chosen to feed the system with, and, where it crosses the different static mixer curves, the coordinates of power input can be found. This information can be used to identify the corresponding $d_{32}$ and Y (Figure 10) at the given power input. For the case study 1 (Figure 11a), the chosen energy allows the system to operate in the confident working zone for the 12 elements KMS and SMX+ and in the inefficient working zone for the other two configurations. The corresponding values of $d_{32}$ and Y are shown in the table in Figure 11a.

Theoretically, it can be argued that if the energy input to the system is the same, the final $d_{32}$ should be similar for different geometries. In the efficient working zone, the achieved results are very similar, suggesting that this approach could be applied to understand the optimal process conditions and predict the performance of a motionless mixing system. In the inefficient zone, the values of the two different geometries differ greatly as expected. To further test the validity of this methodology, a second case is presented in Figure 11b, in which the energy value is chosen to be in the efficient working zone for all devices. The values of $d_{32}$ and Y reported are very similar to each other and this confirms that, regardless of the chosen device, given a fixed energy input, a certain $d_{32}$ can be achieved if working in the efficiency zone.

## Conclusions

A novel approach for the characterisation of in-situ DSD measurement of O-W emulsion is presented. Optical and PLIF measurements and image analysis were used to determine the DSD of oil droplets in water as they formed at the inlet and at the outlet of different static mixer geometries and lengths. Consistent instabilities were observed for all configurations at *Re* above 6000. Existing models were tested which showed good agreement with the experimental data in stable conditions, but poor agreement in the unstable conditions. The acquired data were used to determine the optimal process conditions using an approach based on a self-developed energy model which allows the coupling of energy consumption and drop size distribution.

**Acknowledgments**

Special thanks to the school of Chemical Engineering at University of Birmingham (UK) for supporting this work and to Prof. Mark Simmons and Dr. Richard Greenwood for invaluable help and advice. We also thanks Dr S. Antani for the help during the revision process. This research did not receive any specific grant from funding agencies in the public, commercial, or not-for-profit sectors.

## References


[1] V. Đorđević *et al.*, 'Trends in Encapsulation Technologies for Delivery of Food Bioactive Compounds', *Food Eng. Rev.*, vol. 7, no. 4, pp. 452–490, Dec. 2015.

[2] J. Hategekimana, M. V. M. Chamba, C. F. Shoemaker, H. Majeed, and F. Zhong, 'Vitamin E Nanoemulsions by Emulsion Phase Inversion: Effect of Environmental Stress and Long-term Storage On Stability and Degradation In Different Carrier Oil Types.', *Colloids Surf. Physicochem. Eng.*, vol. 483, pp. 70–80, 2015.

[3] M. B. Munk and M. L. Andersen, 'Partial coalescence in emulsions: The impact of solid fat content and fatty acid composition', *Eur. J. Lipid Sci. Technol.*, vol. 117, no. 10, pp. 1627–1635, Oct. 2015.

[4] M. Obando, A. Papastergiadis, S. Li, and B. De Meulenaer, 'Impact of Lipid and Protein Co-oxidation on Digestibility of Dairy Proteins in Oil-in-Water (O/W) Emulsions', *J. Agric. Food Chem.*, vol. 63, no. 44, pp. 9820–9830, Nov. 2015.

[5] A. M. Pintor, R. S. Souza, V. J. Vilar, C. M. Botelho, and R. A. Boaventura, 'The role of emulsion properties and stability in vegetable oil uptake by regranulated cork sorbents', *J. Chem. Technol. Biotechnol.*, vol. 90, no. 9, pp. 1601–1610, Sep. 2015.

[6] Z. Wang, M. A. Neves, H. Isoda, and M. Nakajima, 'Preparation and Characterization of Micro/Nano-emulsions Containing Functional Food Components ⋆ ', p. 15, 2015.

[7] C. Cramer, P. Fischer, and E. . J. Windhab, 'Drop formation in a co-flowing ambient fluid', *Chem. Eng. Sci.*, vol. 59, no. 15, pp. 3045–3058, 2004.

[8] T. F. Tadros, 'Emulsion Formation, Stability, and Rheology', in *Emulsion Formation and Stability*, Wiley-Blackwell, 2013, pp. 1–75.

[9] M. Ruthven, K. Robin Ko, R. Agarwal, and J. P. Frampton, 'Microscopic evaluation of aqueous two-phase system emulsion characteristics enables rapid determination of critical polymer concentrations for solution micropatterning', *Analyst*, vol. 142, no. 11, pp. 1938–1945, 2017.

[10] T. Lemenand, C. Habchi, D. Della Valle, J. Bellettre, and H. Peerhossaini, 'Mass transfer and emulsification by chaotic advection', *Int. J. Heat Mass Transf.*, vol. 71, pp. 228–235, Apr. 2014.

[11] T. Tadros, P. Izquierdo, J. Esquena, and C. Solans, 'Formation and stability of nano-emulsions', *Adv. Colloid Interface Sci.*, vol. 108–109, pp. 303–318, May 2004.

[12] I. Capek, 'Degradation of kinetically-stable o/w emulsions', *Adv. Colloid Interface Sci.*, vol. 107, no. 2–3, pp. 125–155, Mar. 2004.

[13] P. Fischer and P. Erni, 'Emulsion drops in external flow fields — The role of liquid interfaces', *Curr. Opin. Colloid Interface Sci.*, vol. 12, no. 4, pp. 196–205, Oct. 2007.

[14] N. Kiss *et al.*, 'Formation of O/W emulsions by static mixers for pharmaceutical applications', *Chem. Eng. Sci.*, vol. 66, pp. 5084–5094, 2011.

[15] S. W. T. F.R.S, 'XLVI. Hydrokinetic solutions and observations', *Lond. Edinb. Dublin Philos. Mag. J. Sci.*, vol. 42, no. 281, pp. 362–377, Nov. 1871.

[16] V. Dorfner, J. Domnick, F. Durst, and R. Kohler, 'VISCOSITY AND SURFACE TENSION EFFECTS IN PRESSURE SWIRL ATOMIZATION', *At. Sprays*, vol. 5, no. 3, 1995.

[17] P. K. Das, J. Legrand, P. Morançais, and G. Carnelle, 'Drop breakage model in static mixers at low and intermediate Reynolds number', *Chem. Eng. Sci.*, vol. 60, no. 1, pp. 231–238, Jan. 2005.

[18] F. A. Streiff, P. Mathys, and T. U. Fischer, 'New fundamentals for liquid-liquid dispersion using static mixers', *Réc Prog Gén Proc*, vol. 11, pp. 307–314, 1997.

[19] R. K. Thakur, C. Vial, K. D. P. Nigam, E. B. Nauman, and G. Djelveh, 'Static Mixers in the Process Industries—A Review', *Chem. Eng. Res. Des.*, vol. 81, no. 7, pp. 787–826, Aug. 2003.
[20] S. Ferrouillat, P. Tochon, C. Garnier, and H. Peerhossaini, 'Intensification of heat-transfer and mixing in multifunctional heat exchangers by artificially generated streamwise vorticity', *Appl. Therm. Eng.*, vol. 26, no. 16, pp. 1820–1829, Nov. 2006.
[21] A. Ghanem, T. Lemenand, D. Della Valle, and H. Peerhossaini, 'Static mixers: Mechanisms, applications, and characterization methods – A review', *Chem. Eng. Res. Des.*, vol. 92, no. 2, pp. 205–228, 2014.
[22] J. Legrand, P. Morancais, and G. Carnelle, 'Liquid-liquid dispersion in an SMX-Sulzer static mixer', *Chem. Eng. Res. Des.*, vol. 79, no. A8, pp. 949–956.
[23] F. Theron and N. L. Sauze, 'Comparison between three static mixers for emulsification in turbulent flow', *Int. J. Multiph. Flow*, vol. 37, no. 5, pp. 488–500, Jun. 2011.
[24] E. Lobry, F. Theron, C. Gourdon, N. Le Sauze, C. Xuereb, and T. Lasuye, 'Turbulent liquid–liquid dispersion in SMV static mixer at high dispersed phase concentration', *Chem. Eng. Sci.*, vol. 66, no. 23, pp. 5762–5774, Dec. 2011.
[25] F. Alberini, M. J. H. Simmons, A. Ingram, and E. H. Stitt, 'Assessment of different methods of analysis to characterise the mixing of shear-thinning fluids in a Kenics KM static mixer using PLIF', *Chem. Eng. Sci.*, vol. 112, pp. 152–169, Jun. 2014.
[26] L. Liu, O. K. Matar, C. J. Lawrence, and G. F. Hewitt, 'Laser-induced fluorescence (LIF) studies of liquid–liquid flows. Part I: Flow structures and phase inversion', *Chem. Eng. Sci.*, vol. 61, no. 12, pp. 4007–4021, Jun. 2006.
[27] F. Alberini, D. Dapelo, R. Enjalbert, Y. Van Crombrugge, and M. J. H. Simmons, 'Influence of DC electric field upon the production of oil-in-water-in-oil double emulsions in upwards mm-scale channels at low electric field strength', *Exp. Therm. Fluid Sci.*, vol. 81, pp. 265–276, Feb. 2017.
[28] A. Buffo and V. Alopaeus, 'Experimental determination of size distributions: analyzing proper sample sizes', *Meas. Sci. Technol.*, vol. 27, no. 4, p. 045301, 2016.
[29] P. Walstra, 'Principles of emulsion formation', *Chem. Eng. Sci.*, vol. 48, no. 2, pp. 333–349, Jan. 1993.
[30] A. N. Kolmogorov, 'On the breakage of drops in a turbulent flow', *Dokl Akad Nauk SSSR*, vol. 66, pp. 825–828, 1949.
[31] M. Ashar, D. Arlov, F. Carlsson, F. Innings, and R. Andersson, 'Single droplet breakup in a rotor-stator mixer', *Chem. Eng. Sci.*, vol. 181, pp. 186–198, May 2018.
[32] B. P. Binks, F. Adams, and P. Walstra, 'Modern Aspects of Emulsion'. Science Royal Society of Chemistry, 1998.
[33] N. B. Raikar, S. R. Bhatia, M. F. Malone, and M. A. Henson, 'Experimental studies and population balance equation models for breakage prediction of emulsion drop size distributions', *Chem. Eng. Sci.*, vol. 64, no. 10, pp. 2433–2447, May 2009.
[34] N. Vankova, S. Tcholakova, N. D. Denkov, I. B. Ivanov, V. D. Vulchev, and T. Danner, 'Emulsification in turbulent flow: 1. Mean and maximum drop diameters in inertial and viscous regimes', *J. Colloid Interface Sci.*, vol. 312, no. 2, pp. 363–380, Aug. 2007.
[35] C. Xing, T. Wang, K. Guo, and J. Wang, 'A unified theoretical model for breakup of bubbles and droplets in turbulent flows', *AIChE J.*, vol. 61, no. 4, pp. 1391–1403, Apr. 2015.
[36] A. Håkansson, H. H. Mortensen, R. Andersson, and F. Innings, 'Experimental investigations of turbulent fragmenting stresses in a rotor-stator mixer. Part 1. Estimation of turbulent stresses and comparison to breakup visualizations', *Chem. Eng. Sci.*, vol. 171, pp. 625–637, Nov. 2017.

[37] M. Konno, M. Aoki, and S. Saito, 'Scale effect on breakup process in liquid-liquid agitated tanks', *J. Chem. Eng. Jpn.*, vol. 16, no. 4, pp. 312–319, Aug. 1983.
[38] J. O. Hinze, 'Fundamentals of the hydrodynamic mechanism of splitting in dispersion processes', *AIChE J.*, vol. 1, no. 3, pp. 289–295, Sep. 1955.
[39] T. Lemenand, D. Della Valle, Y. Zellouf, and H. Peerhossaini, 'Droplets formation in turbulent mixing of two immiscible fluids in a new type of static mixer', *Int. J. Multiph. Flow*, vol. 29, no. 5, pp. 813–840, May 2003.
[40] S. Middleman, 'Drop size distributions produced by turbulent pipe flow of immiscible fluids through a static mixer', *Ind. Eng. Chem. Process Dev*, vol. 13, pp. 78–83, 1974.
[41] P. D. Berkman and R. V. Calabrese, 'Dispersion of viscous liquids by turbulent flow in a static mixer', *AIChE J.*, vol. 34, no. 4, pp. 602–609, Apr. 1988.
[42] F. A. Streiff, S. Jaffer, and G. Schneider, 'Design and application of motionless mixer technology', in *International Symposium on Mixing in Industrial Processes*, Osaka, 1999.
[43] D. Poncelet and R. J. Neufeld, 'Fundamentals of dispersion in encapsulation technology.', in *Immobilized Cells: Basics and applications*, Elsevier Science, 1996, pp. 47–54.
[44] L. Fradette, B. Brocart, and P. A. Tanguy, 'Comparison of Mixing Technologies for the Production of Concentrated Emulsions', *Chem. Eng. Res. Des.*, vol. 85, no. 11, pp. 1553–1560, Jan. 2007.
[45] K. Hirech, A. Arhaliass, and J. Legrand, 'Experimental Investigation of Flow Regimes in an SMX Sulzer Static Mixer', *Ind. Eng. Chem. Res.*, vol. 42, no. 7, pp. 1478–1484, Apr. 2003.
[46] O. Reynolds, 'An experimental investigation of the circumstances which determine whether the motion of water in parallel channels shall be direct or sinuous and of the law of resistance in parallel channels', *Philos. Trans. R. Soc.*, 1883.

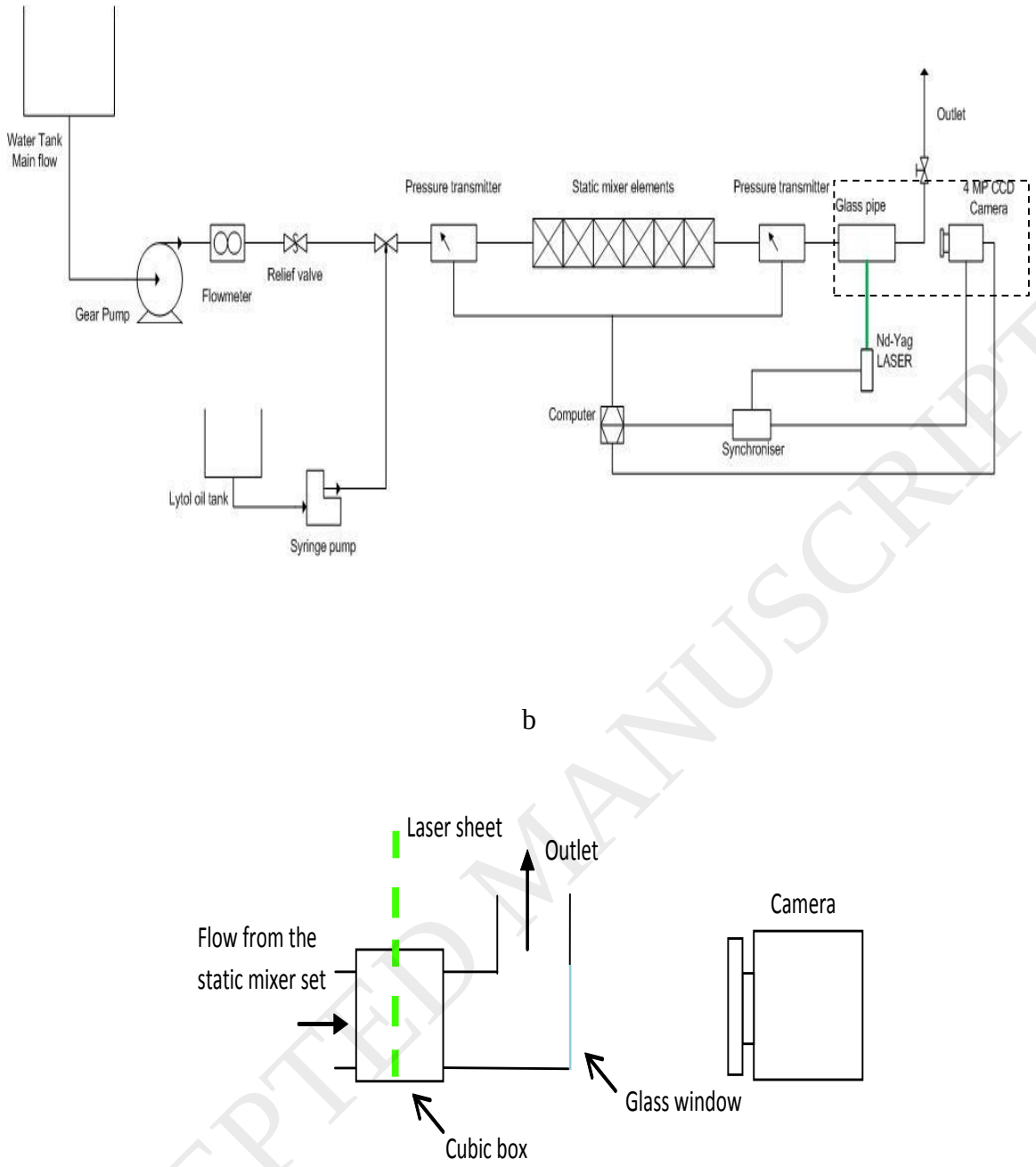


*Figure 1: (a) Schematic rig and (b) zoom of the dashed rectangle including Tee Piece window for PLIF measurements.*

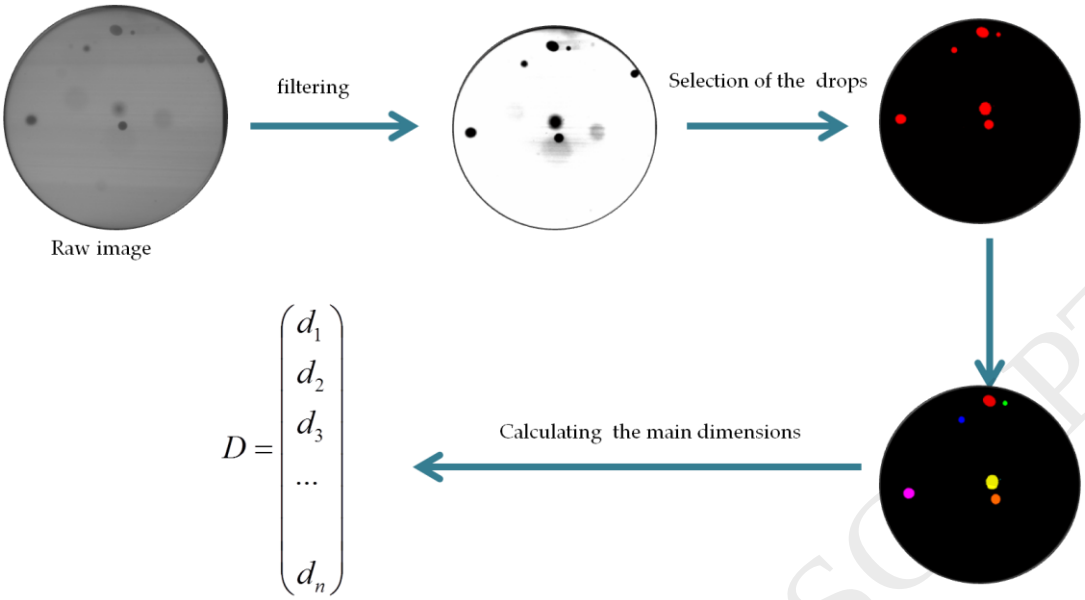


*Figure 2: The four main steps used to obtain particle size measurements from PLIF raw images*

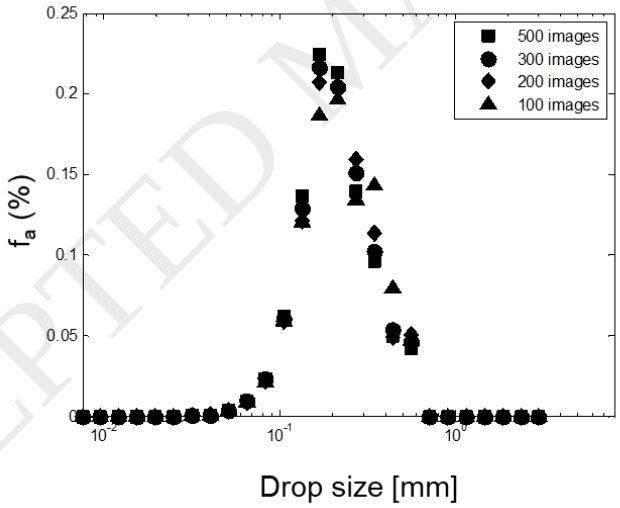


*Figure 3: The repeatability and the consistence of DSD plots from image analysis for 6 elements SMX+ at Re=6000.*

| | Time step 1 – drop formation | Time step 2 – elongation and breakage | Time step 3 – Breakage of the satellite | Time step 4 – Formed droplets |
|---|---|---|---|---|
| (a) |  |  |  |  |
| (b) |  |  |  |  |
| (c) |  |  |  |  |

*Figure 4: Binary images of droplet formation at different time steps for (a) Re=5000, (b) Re=9500 and (c) Re=12000*

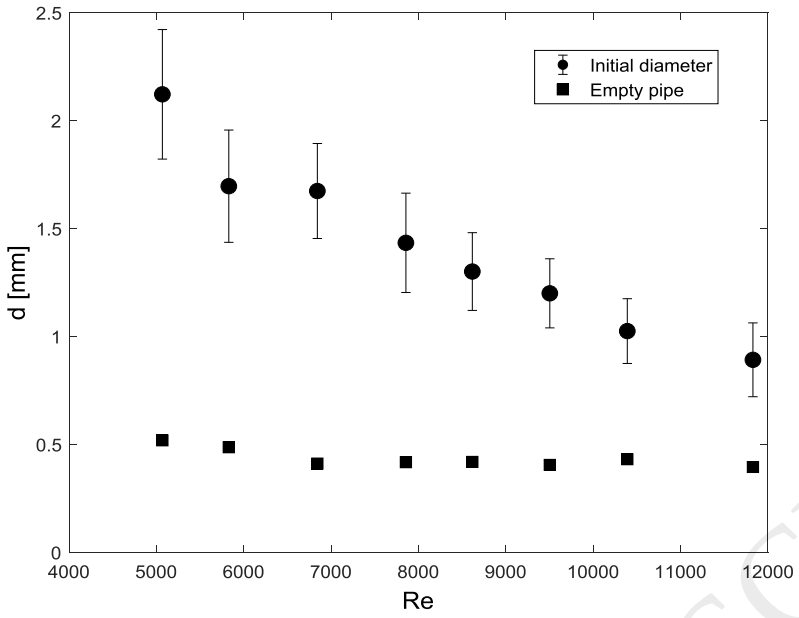


*Figure 5: Initial diameters ($d=d_{IN}$) versus Re at the inlet and $d=d_{32}$ at the end of an empty pipe.*

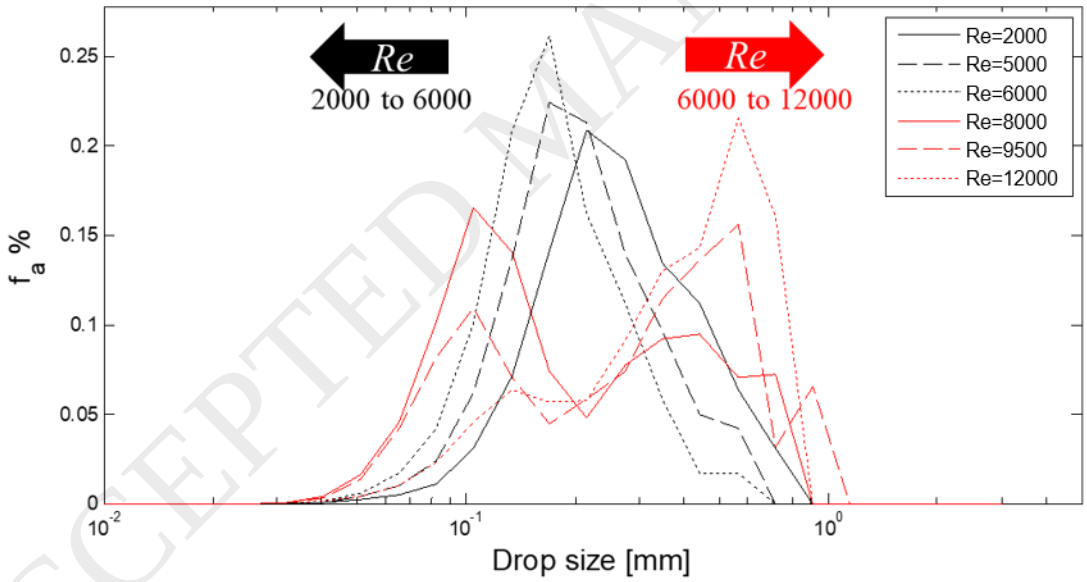


*Figure 6: Drop size distribution at different Re ranging from 2000 to 12000 for the 12 elements SMX+.*

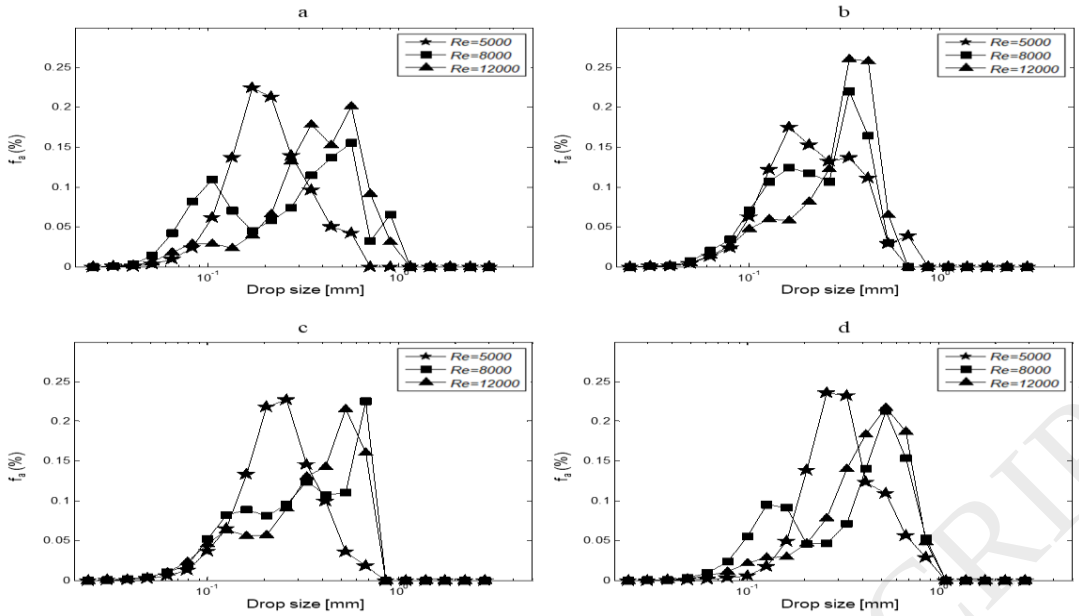


*Figure 7: Drop size distribution at different Re ranging from 5000 to 12000 for (a)12 elements SMX+, (b)12 elements KMS, (c) 6 elements SMX+ and (d) 6 elements KMS.*

a

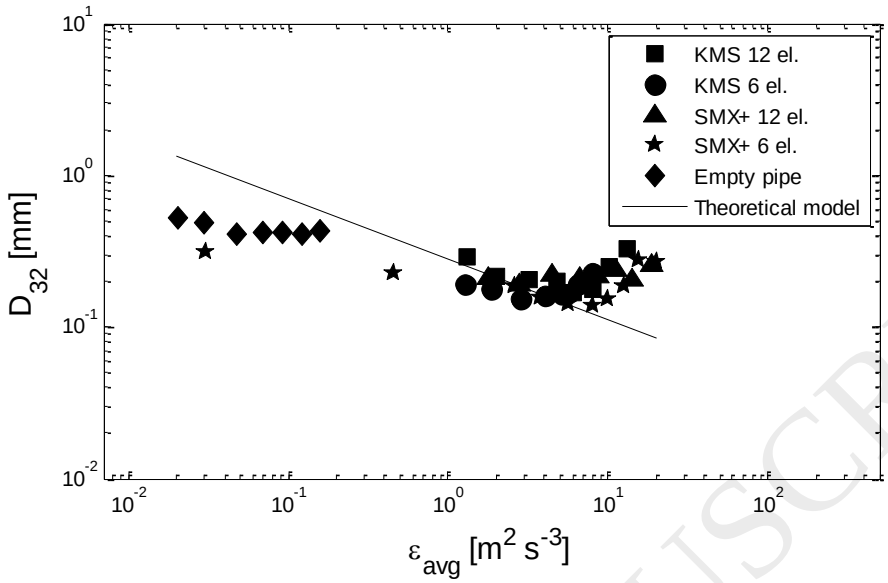


b

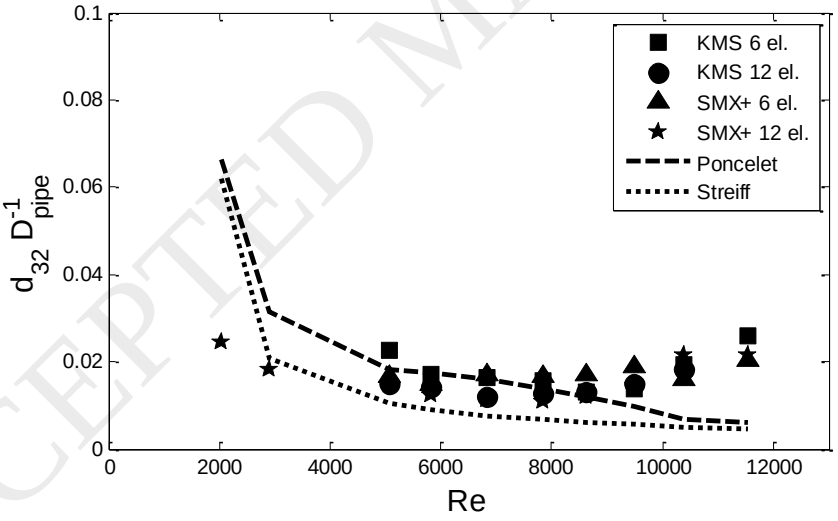


*Figure 8: (a)Experimental $d_{32}$ versus energy dissipation (calculated form Eq. (5)) and Hinze model fitting and (b) $d_{32}/D_{pipe}$ versus Re fitted in Streiff and Poncelet models.*

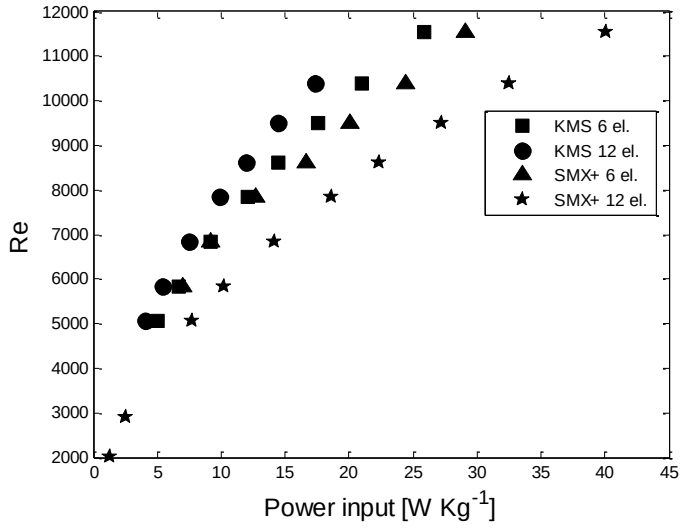


*Figure 9: Power input (calculated form Eq. (17)) versus Re*

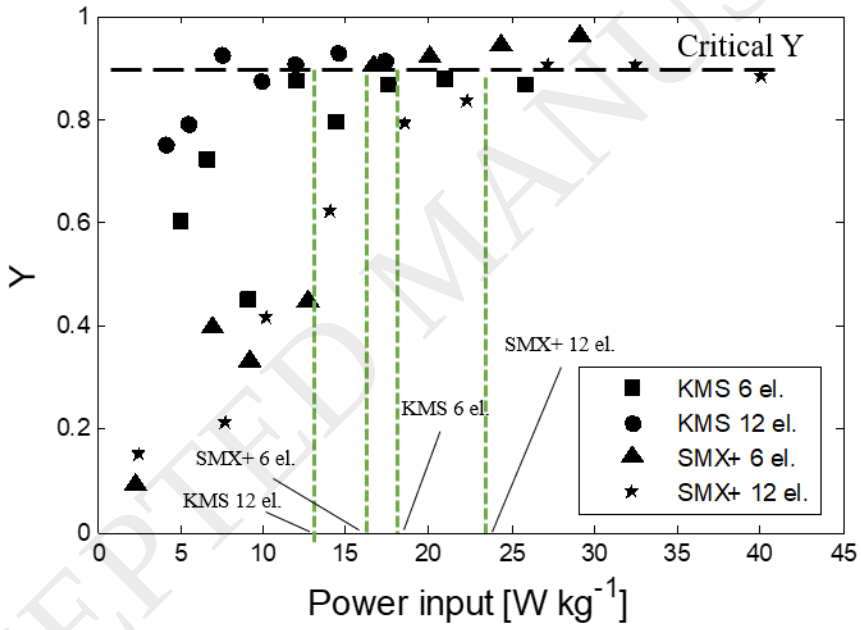


*Figure 10: Breakup efficiency Y versus power input for the different static mixer configurations.*

a

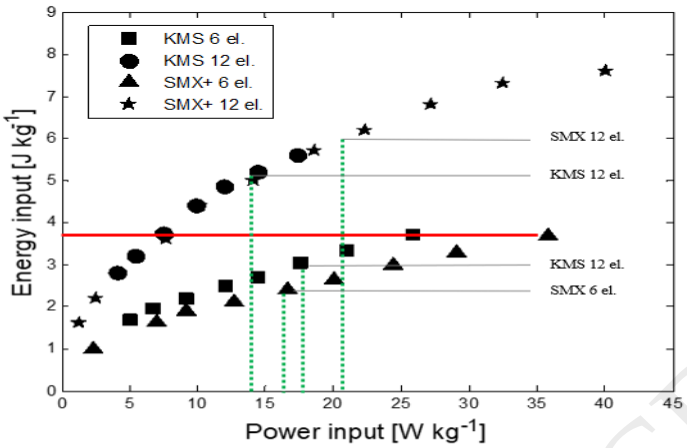


| Configuration | KMS 6 el. | KMS 12 el. | SMX+ 6 el. | SMX+ 12 el. |
|---|---|---|---|---|
| $d_{32}$ [mm] | 0.247 | 0.168 | 0.227 | 0.165 |
| $Y$ | 0.820 | 0.987 | 0.800 | 0.987 |

b

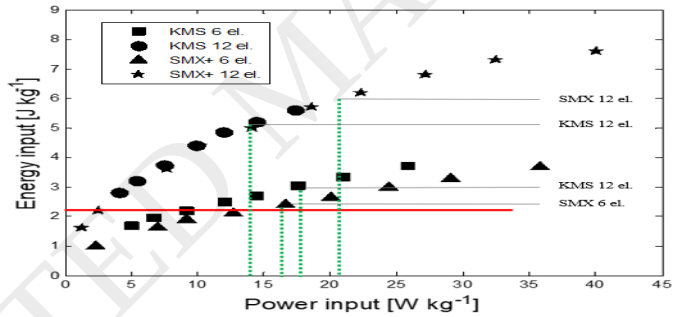


| Configuration | KMS 6 el. | KMS 12 el. | SMX+ 6 el. | SMX+ 12 el. |
|---|---|---|---|---|
| $d_{32}$ [mm] | 0.20 | 0.20 | 0.21 | 0.19 |
| $Y$ | 0.973 | 0.975 | 0.95 | 0.976 |

*Figure 11: (a) Case study 1: a fixed value of 3.8 J per kg of energy input was chosen; this value intercepts the 12 elements SMX+ and KMS within the breakup efficiency of 95 % but not for the 6 elements hence lower efficiency of breakup is expected. (b) case study 2: a fixed value of 2.2 J per kg of energy input was chosen; this value intercept the 12 and 6 elements SMX+ and KMS within the breakup efficiency of 95 % hence similar efficiency of breakup is expected.*

*Table 1. Properties of fluids*

| | Phase | Density [kg $m^{-3}$] | Viscosity (Pa s) | Interface tension ( N/m) |
|---|---|---|---|---|
| Water | Continuous | 997.8 | 0.001 | 0.02267 |
| Lytol oil | Dispersed | 800 | 0.0032 | |

*Table 2 Calculated parameters for Buffo and Alopaeus[28] methodology for the selected velocities.*

| Distribution type | Mono-modal | | | | Bi-modal | |
|---|---|---|---|---|---|---|
| Static Mixer | 6 KMS | 6 SMX+ | 12 KMS | 12 SMX+ | 12 KMS | 12 SMX+ |
| N | 4673.00 | 3467.00 | 9301.00 | 9901.00 | 4269.00 | 5506.00 |
| $\bar{L}$ [mm] | 0.14 | 0.11 | 0.10 | 0.09 | 0.10 | 0.11 |
| $S^2$ | 0.02 | 0.01 | 0.01 | 0.01 | 0.01 | 0.02 |
| $\sigma_{SE}$ | 2.27E-03 | 2.01E-03 | 1.19E-03 | 9.70E-04 | 2.04E-03 | 1.69E-03 |
| $\Delta L$ [mm] | 0.03 | 0.03 | 0.03 | 0.03 | 0.03 | 0.03 |
| Level of confidence | 0.99 | 0.99 | 0.99 | 0.99 | 0.99 | 0.99 |
| $t_\infty$ | 2.33 | 2.33 | 2.33 | 2.33 | 2.33 | 2.33 |
| $N^*$ | 687.80 | 397.32 | 373.26 | 265.13 | 373.37 | 447.95 |

*Table 3. Parameters characterising the flow at different superficial velocities.*

| V | 0.4 | | | 0.54 | | | 0.75 | | | 0.82 | | |
|---|---|---|---|---|---|---|---|---|---|---|---|---|
| | ΔP | ε | Re | Δp | ε | Re | Δp | ε | Re | Δp | ε | Re |
| 12 KMS | 3427 | 1.27 | 5069 | 5693 | 2.85 | 6843 | 9380 | 6.53 | 9504 | 10686 | 8.13 | 10391 |
| 12 SMX+ | 4948 | 2.61 | 5069 | 7957 | 5.67 | 6843 | 12755 | 12.62 | 9504 | 14431 | 15.60 | 10391 |
| 6 KMS | 1762 | 1.31 | 5069 | 3228 | 3.24 | 6843 | 5722 | 7.96 | 9504 | 6631 | 10.09 | 10391 |
| 6 SMX+ | 1707 | 1.80 | 5069 | 3167 | 4.51 | 6843 | 5655 | 11.19 | 9504 | 6564 | 14.20 | 10391 |